THE JOURNAL OF PHYSICAL CHEMISTRY C
A JOURNAL OF THE AMERICAN CHEMICAL SOCIETY

pubs.acs.org/JPCC

Article

Uphill Anion Pumping through Triangular Nanofluidic Device of Reconstructed Layered Double Hydroxide

Tukhar Jyoti Konch, Trisha Dutta, Arindom Bikash Neog, Raktim Gogoi, and Kalyan Raidongia*

Cite This: J. Phys. Chem. C 2021, 125, 17939–17949

Read Online

ACCESS | Metrics & More | Article Recommendations | Supporting Information

ABSTRACT: Numerous research efforts have been devoted to replicate the functioning of biological ion pumps in nanofluidic devices. Unlike previous reports of cationic pumps, positively charged CoAl layered double hydroxide (CoAl LDH) is exploited here for uphill pumping of anionic species. Nanofluidic membranes prepared by self-assembling exfoliated layers of CoAl LDH exhibit excellent anionic transport characteristics. At the surface-charge-governed regime, the positively charged CoAl LDH membrane (p-LDHM) showed a remarkable OH^- ion conductivity of ~2 mS cm^{-1}. The remarkable mobility of OH^- ions (4×10^{-4} cm^2 V^{-1} S^{-1}) in the atomically thin channel of p-LDHM is attributed to the tiny activation energy (0.09 eV) required for Grotthuss-like hopping of the ions between the positive charges of densely packed CoAl LDH layers. The lamellar p-LDHM was also found to be suitable for energy harvesting via salinity gradient, and a power density up to 0.7 Wm^{-2} was achieved under a 1000-fold concentration gradient. The triangular p-LDHM displays a diode-like nonlinear $I-V$ curve, attributed to a combination of unipolar conductivity of counterions inside the two-dimensional (2D) nanochannels and geometrical asymmetry. The triangular p-LDHM pumps anions against the concentration gradient (up to 1000-fold), under fluctuating external potentials with a mean value of zero.

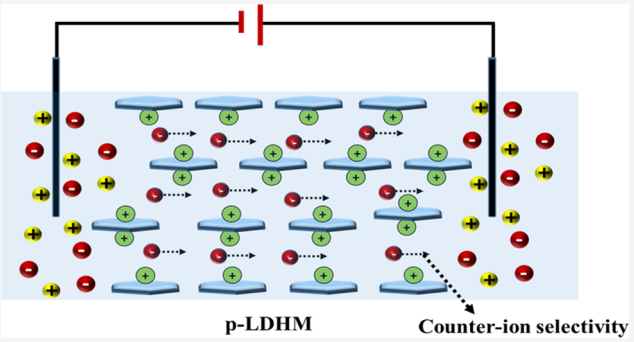

INTRODUCTION

Ion pumps with intricate transport properties play critically important roles in various physiological functions of living organisms. For example, the specific internal composition of the biological ion channels is regulated by the Na^+/K^+ ion pump, which is essential for maintaining osmotic equilibrium and membrane potential of cells.[1,2] Similarly, plasma membrane Ca^{2+} ATPase (PMCA) is vital for regulating Ca^{2+}-ion concentration within eukaryotic cells.[3,4] The energy needed for the regulation of different ion pumps is supplied through sources like light, redox chemicals, and ATP.[5,6] Inspired by the exceptional properties of the biological ion pumps, several efforts have been devoted to fabricating their artificial counterparts.[7−10] Bio-inspired synthetic pumps capable of transporting ions/molecules in the uphill direction in a highly selective manner have great relevance to futuristic applications in areas like bio-sensing, environmental studies, and energy harvesting.[11−13] So far, most of the studies related to the biomimetic ion pumps are limited to only cation pumping. To the best of our knowledge, no progress has been made toward developing artificial ion pumps capable of transporting anions in the uphill direction. Here, we report the fabrication of an ion pump that can push anions toward a higher-concentration chamber with the help of a fluctuating electric field with a mean value of zero.

The demonstration of the feasibility of creating an unprecedentedly massive array of nanofluidic channels by restacking exfoliated sheets of layered material provided a macroscopic platform to study the nanoscale phenomena occurring at the liquid state.[14] By the virtue of its unique advantages such as cost-effectiveness, scalability, ease of modifications, and high-flux, reconstructed layered materials initiated a new era of nanofluidic studies. It is also creating novel avenues to exploit nanofluidic phenomena for various practical applications like harvesting of electrokinetic energy, ultrafiltration, biomedical analysis, seawater desalination, and DNA sequencing.[15−20] The synchronous growth in the research related to the novel two-dimensional (2D) nanomaterials further boosted the research in two-dimensional nanofluidics. After the initial demonstration with graphene oxide, numerous other layered materials such as h-BN, clay minerals, transition-metal dichalcogenide, Mxenes, and carbon nitride were utilized to create nanofluidic devices with unique

Received: April 7, 2021
Revised: July 27, 2021
Published: August 5, 2021

https://doi.org/10.1021/acs.jpcc.1c03118
J. Phys. Chem. C 2021, 125, 17939−17949

characteristics, mostly via reconstruction of their respective exfoliated layers.[21−25] Remarkably, to date, most of these nanofluidic studies are limited to only cation-selective nanochannels. However, utilization of both the cation- and anion-selective membranes is desired to enhance the operational performance of several futuristic applications such as osmotic power generation, seawater desalination, and regulated ionic/molecular transportations. Several indirect approaches like reactive surface groups (COOH or OH) modification of the parent cation-selective 2D sheets and intercalation of cationic polymers were adopted to imbue anion selectivity to the nanofluidic channels, and subsequently both the parent and modified nanofluidic channels were utilized with synchronization to achieve better performance in osmotic energy harvesting and seawater desalination.[26−29] The application of foreign materials/molecules not only involves additional chemical processes but also disturbs the well-defined 2D structure of the nanochannels. Along with decreasing nanofluidic confinements, it also exerts adverse effects on the mechanical, chemical, and thermal stabilities of the nanofluidic membranes.[30] Therefore, efforts have been devoted to prepare anion-conductive materials using layered double hydroxide-based materials.[31,32] In the present work, we have utilized the inherent positive charges of the cationic Co-Al layered double hydroxide (CoAl LDH) to fabricate anion-selective nanofluidic devices. The lamellar membrane of CoAl LDH was exploited for preparing a triangular ion pump capable of transporting anions against the concentration gradient, as well as to fabricate salinity gradient-driven energy harvesting devices.

Layered double hydroxides (LDHs) represent a class of lamellar compounds with a general formula of $[M_{1-x}^{2+}M^{3+}_{x}(OH)_2]^{x+}\cdot[A_{n-x/n}].mH_2O$, where M represents metal cations and A represents anions.[33] Typically, LDHs consist of alternatively staked positively charged brucite-like host layers and charge-balancing hydrated exchangeable anions located in the interlayer gallery. In the brucite host layers, the metal cations occupy the centers of the edge-sharing octahedra, whose vertexes contain hydroxide ions that connect to form infinite 2D sheets. The charges of the brucite-like layers arise from the isomorphous substitution of divalent metal ions with trivalent ones.[34] The positive charges on the host layers attract the water molecules and provide an extensive network of hydrogen bonding along the 2D surface. The hydrogen-bonding network facilitates swift conduction of OH^- ions through the rapid cleavage reconstruction process of hydrogen bonds.[31,32] In clear contrast to typical layered materials, LDHs like CoAl LDH are composed of positively charged host layers with interlayer spaces occupied by charge-balancing anions. The lamellar crystallites of LDH can be exfoliated into atomically thin 2D sheets with a high density of positive charges.

Materials. Cobalt chloride hexahydrate, aluminum chloride hexahydrate, urea, sodium chloride, potassium chloride, potassium hydroxide, sodium hydroxide, sodium fluoride, sodium sulfate, and hydrochloric acid were purchased from Merck. Formamide and *N*,*N*-dimethylformamide were purchased from SRL Pvt. Ltd., India.

Characterization. CoAl LDH nanosheets were characterized by a field emission transmission electron microscope (FETEM) (JEOL, model: 2100F), a field emission scanning electron microscope (Make: Zeiss, model: Sigma), and an atomic force microscope (AFM) (Make: Oxford; model: Cypher). The cross sections of the membranes were examined by a field emission scanning electron microscope (Make: Zeiss, model: Sigma). Ion intercalation and exfoliation of the bulk LDH platelets were investigated with the help of a Fourier transform infrared (FTIR) spectrometer (Maker: PerkinElmer; model: Spectrum Two) and X-ray diffraction studies (Rigaku, model: Micromax-007HF instrument). ζ-Potential measurements were done with a ζ-potential analyzer (Malvern Zetasizer Nano ZS90). Energy-dispersive X-ray analysis was performed with a field emission scanning electron microscope (FESEM) (Zeiss, model: Sigma).

METHODS

Synthesis of CoAl LDH. The hexagonal CoAl LDH-Co_3^{2-} platelets were synthesized following a previously developed soft chemical procedure from a mixed solution of $CoCl_2\cdot6H_2O$ and $AlCl_3\cdot6H_2O$, using urea [$CO(NH_2)_2$] as a hydrolysis agent. Typically, $CoCl_2\cdot6H_2O$, $AlCl_3\cdot6H_2O$, and urea were dissolved in a 1 L round-bottom flask where the final concentration of the reactants is maintained as 10, 5, and 35 mM respectively. Then, the final mixture was refluxed for 48 h in the presence of nitrogen atmosphere under constant stirring. The resulting pink solid mass was filtered, washed with deionized water and ethanol, and air-dried at room temperature. Decarbonation and anion exchange into Cl^- forms (CoAl LDH-Cl^-) were mediated by a salt-acid treatment of 1 g of LDH with a 1 L mixed solution of 1 M NaCl and 3.3 mM HCl under mechanical stirring for a duration of 12 h.

Exfoliation of CoAl LDH. Delamination/exfoliation of CoAl LDH-Cl^- platelets into 2D sheets are done in a 1:1 mixture of formamide and *N*,*N*-dimethylformamide (DMF) under mechanical shaking for a duration of 48 h. Exfoliation of LDH into a few layers of 2D sheets is unlikely to achieve in aqueous environment as the interlayer water molecules form dense hydrogen-bonding network to the hydroxyl groups of the LDH host as well as with the coordinated interlayer anionic guests. Therefore, an equimolar mixture of formamide and DMF is used as the dispersing medium as well as the exfoliating agent. Owing to their highly polar nature, formamide molecules enter the interlayer galleries of LDH lamellas replacing the interlayer water molecules, where its carbonyl group would have strong interaction with the LDH host. Simultaneously the NH_2 moieties of the formamide molecules having lesser extent of hydrogen bonding compared to that of the hydroxide group may not be able to build a strong interaction with the interlayer guest anions. Accordingly, once the replacement of water molecules for formamide takes place, it weakens the interlayer force of attraction disrupting the strong hydrogen-bonding network, thereby inducing delamination. The role of using DMF as an additional exfoliating agent is to impede the strong hydrogen-bonding network in between the interlayers of the LDH framework, thereupon inducing better delamination.

Surface-Charge-Governed Ionic Transport. Nanofluidics devices of p-LDHM were fabricated by encapsulating rectangular strips of known dimensions into the freshly prepared poly(dimethylsiloxane) (PDMS) elastomer. To expose the nanochannel networks to different electrolyte solutions, two holes (~0.4 mL) were cut open through the fully cured PDMS stub at either end of rectangular strips. Ag/AgCl electrodes connected to the terminals of a Keithley source meter (model 2450) were immersed in the reservoirs filled with electrolytes at both ends of the strip to measure the ionic current. Representative $I-V$ curves for the LDH strips

https://doi.org/10.1021/acs.jpcc.1c03118
J. Phys. Chem. C 2021, 125, 17939−17949

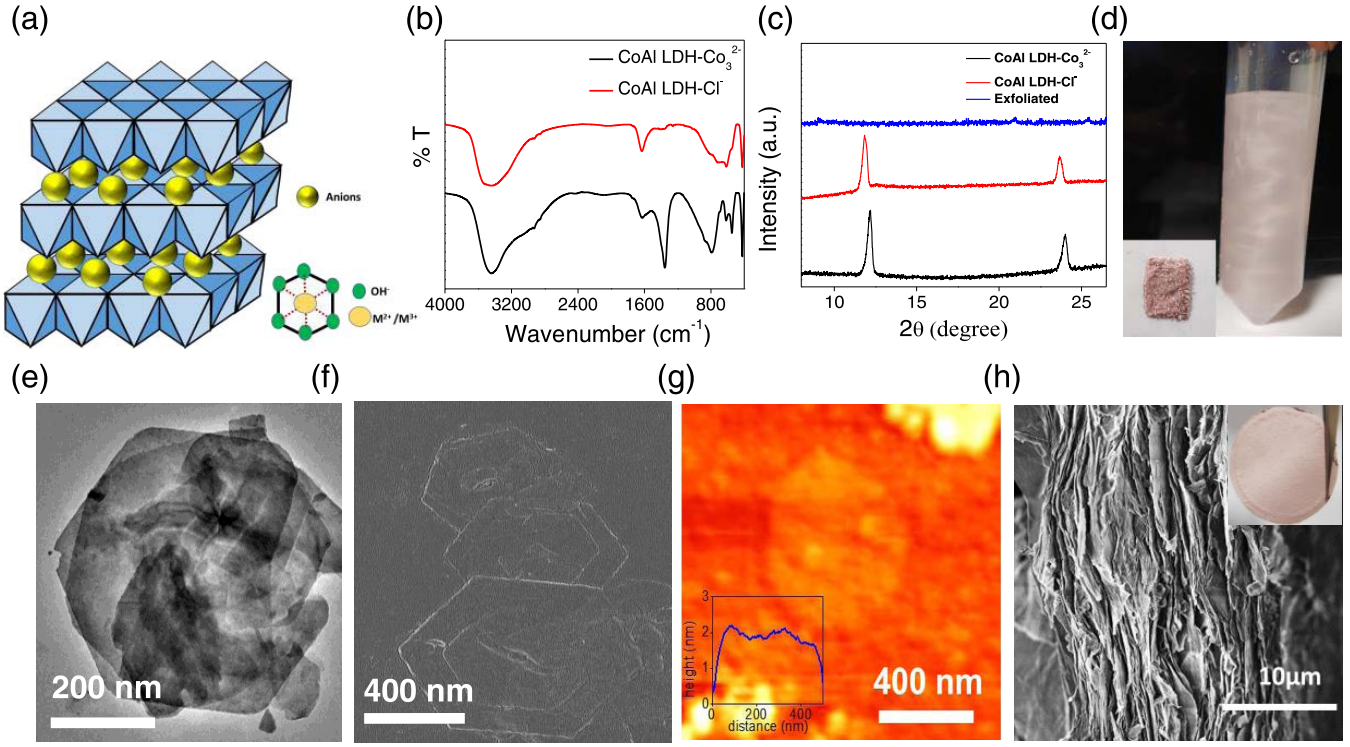

Figure 1. Characterization of CoAl LDH: (a) Schematic representation of the lamellar structure of layered double hydroxide (LDH). (b) Comparison of FT-IR spectra of CoAl LDH-Co_3^{2-} and CoAl LDH-Cl^-; disappearance of the peaks at 1360 and 795 cm^{-1} signifies the removal of intercalated carbonate ions in the chloride-exchanged product. (c) PXRD pattern of powdered CoAl LDH-Co_3^{2-}, CoAl LDH-Cl^-, and exfoliated flakes of CoAl LDH-Cl^- in formamide. (d) Digital photo of the colloidal dispersion of CoAl LDH-Cl^- in formamide (inset shows a photo of CoAl LDH-Cl^- powder). (e) FETEM, (f) FESEM, and (g) AFM images of exfoliated CoAl LDH flake. (h) Cross-sectional FESEM images of the reconstructed LDH membrane; the inset shows the digital image of a freestanding LDH membrane.

were recorded at different electrolyte concentrations ranging from 10^{-6} to 1 M by sweeping voltage from −1 to +1 V across each strip. Conductivity calculations were done using the following equation: $C = G \times$ cell constant, where C is the conductivity and G is the conductance.

RESULTS AND DISCUSSION

The hexagonal CoAl LDH-CO_3^{2-} platelets were synthesized from a mixed solution of $CoCl_2{\cdot}6H_2O$ and $AlCl_3{\cdot}6H_2O$ using urea [$CO(NH_2)_2$] as a hydrolysis agent, adopting a method reported earlier.[35] The formation of LDH material in CO_3^{2-} form was confirmed by recording powder XRD pattern (Figure 1c) of the material. The XRD reflections were matched with rhombohedral structure of LDH, and the interlayer spacing was calculated as 0.72 nm (003).[36,37] The as-synthesized CoAl LDH-CO_3^{2-} platelets were transformed into CoAl LDH-Cl^- through an anion exchange process performed with an aqueous solution of HCl and NaCl under vigorous mechanical stirring.[32] Successful decarbonation process was confirmed by the absence of strong bands at 1360 and 795 cm^{-1} corresponding to the ν_3 vibration and bending modes of CO_3^{2-} FT-IR spectra (Figure 1b).[35] Moreover, in the chloride-exchanged form, the interlayer spacing of LDH was found to be 0.74 nm, slightly higher than that of carbonate form. The decarbonated CoAl LDH-Cl^- platelets were further exfoliated into 2D sheets by stirring the sample in a 1:1 mixture of formamide and *N*,*N*-dimethylformamide (DMF) for 48 h. The formamide treatment transformed the color of the as-prepared CoAl LDH-Cl^- platelets into a pink dispersion (1 mg/mL) (Figure 1d), indicating occurrence of the delamination process. The successful delamination process of the platelets was confirmed by the absence of the sharp basal reflections of the parent CoAl LDH-Cl^- in the powder XRD pattern.[37] Transmission electron microscopy (TEM) and field emission scanning electron microscopy (FESEM) investigation on the drop-cast aqueous dispersion of exfoliated LDH sample displayed presence of hexagonal 2D sheets with lateral dimensions in the range of 1−1.5 μm. Representative images are shown in Figure 1e,1f, respectively. In the atomic force microscopy (AFM) examination, the thicknesses of the exfoliated sheets were found to be in the range of 2−4 nm. A typical AFM image along with the corresponding height profile of an exfoliated CoAl LDH-Cl^- sheet is shown in Figure 1g. The ζ-potential measurements of the aqueous dispersion revealed that the surface of the nanosheets is composed of +29 mV charges. The positive charges in CoAl LDH-Cl^- sheets are attributed to the isomorphous substitution of a part of the divalent metal ions with trivalent ones; details are discussed in Supporting Figure S1.

To create ultraconfined spaces for nanofluidic transportation of anions, a dispersion (1 mg/mL) of exfoliated CoAl LDH-Cl^- in formamide was vacuum-filtered through a poly(tetrafluoroethylene) (PTFE) filtration membrane. Due to its large aspect ratio, during the vacuum-assisted filtration process, nanosheets of CoAl LDH-Cl^- were self-assembled in a lamellar manner, creating a positively charged LDH membrane (p-LDHM). Upon air-drying for 24 h, under ambient conditions, the p-LDHM got detached by itself from the PTFE membrane. The freestanding nature of the p-LDHM is evident from the digital photo shown in Figure 1h (inset). The pXRD pattern in

https://doi.org/10.1021/acs.jpcc.1c03118
J. Phys. Chem. C 2021, 125, 17939−17949

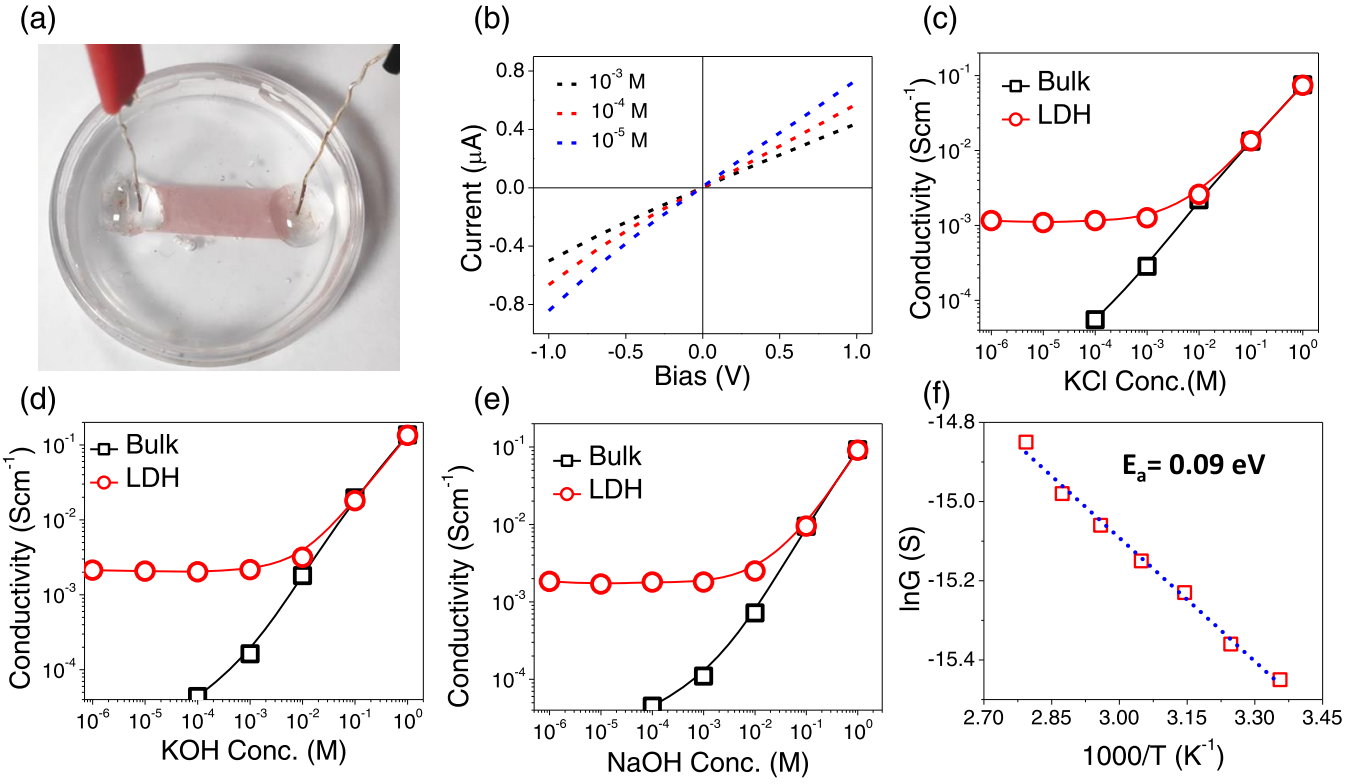

Figure 2. Nanofluidic study through p-LDHM: (a) Digital image of a p-LDHM based nanofluidic device. (b) $I-V$ curves recorded with a nanofluidic device made from a rectangular strip of p-LDHM after soaking the same in aqueous KCl solutions of different concentrations. Ionic conductivity as a function of concentration for aqueous solutions of (c) KCl, (d) KOH, and (e) NaOH. (f) Arrhenius plot of hydroxyl ion conductivity.

Supporting Figure S2 suggests that periodic stacking of CoAl LDH-Cl^- platelets was regained in their reconstructed membrane. The lamellar restacking of the exfoliated 2D sheets in the p-LDHM is also revealed by the cross-sectional FESEM image shown in Figure 1h. Upon soaking in water for 2 h, the interlayer spacing of the LDH membrane was found to be increased from 0.74 to 0.86 nm, confirmed by the in situ XRD experiment (Supporting Figure S2). As the thickness of an individual CoAl LDH-Cl^- layer is reported to be 0.46 nm, the space available for the nanofluidic transport can be estimated to be around 0.40 nm.

The ionic transportation characteristics of p-LDHM nanochannels were investigated by fabricating nanofluidic devices out of reconstructed LDH membrane. In brief, freestanding p-LDHM (thickness, 40 μm) was cut into rectangular strips of dimensions of 20 mm × 5 mm and immersed into freshly prepared poly(dimethylsiloxane) (PDMS) elastomer solution before curing the same at 60 °C. To expose the p-LDHM strip to desired electrolyte solutions, two reservoirs of about 0.4 mL in volume were carved out at both ends of the PDMS stub (Figure 2a). After hydrating nanofluidic channels with DI water for 24 h, both the reservoirs were filled with electrolyte solutions of known concentration. The ionic current through the p-LDHM nanofluidic device was measured via Ag/AgCl electrodes inserted into the electrolyte solutions placed in the reservoirs. The linearity of the $I-V$ curve measured with aqueous KCl solutions of different concentrations (Figure 2b) confirmed the formation of an interconnected network of the nanochannels. The ionic conductivity values at different electrolyte concentrations were calculated by normalizing the slope of the $I-V$ curves with the overall dimensions (length (l), width (w), and thickness (t) of the rectangular pieces used for the device fabrication). In Figure 2c–e, conductivity values calculated through p-LDHM with aqueous solutions of KCl, KOH, and NaOH are plotted as a function of salt concentration. The freestanding p-LDHM showed the characteristics of surface-charge-governed ionic conductivity, where in the high-concentration regime (0.1–1 M), similar to that of the bulk solution, the conductivity of the LDH nanochannels varied linearly with salt concentration. But in the low-concentration regime (10^{-2}–10^{-6} M), conductivity values did not change 4 orders of magnitude in the electrolyte concentrations, which is in clear contrast to the bulk solution. This peculiar conductivity pattern in the low-concentration regime is attributed to the overlapping of Debye lengths of the channel surfaces. Under such circumstances, the intrinsic surface-charge density of the walls of the channels preferentially draws counterions, and the concentration of the counterions inside the nanochannels is governed by the density of the surface charge, not by the concentration of the electrolytes present in the reservoirs.[14,22] The occurrence of surface-charge-governed ionic conductivity also indicates the absence of large macroscopic voids in the lamellar membrane.

The dominance of the anions in the nanofluidic conductivity of the p-LDHM-based devices was verified by replacing the electrolyte KCl with KOH. Substitution of Cl^- with OH^-, keeping the cationic counterpart (K^+) unaltered, enhanced the conductivity values in the surface-charge-governed regime by a factor of 8 (Figure 2c,2d). A similar replacement of cations from K^+ to Na^+ by keeping the anionic part constant (OH^-) did not alter the conductivity values (Figure 2d,2e). Similarly, the surface-charge-governed ionic conductivity of p-LDHM

https://doi.org/10.1021/acs.jpcc.1c03118
J. Phys. Chem. C 2021, 125, 17939–17949

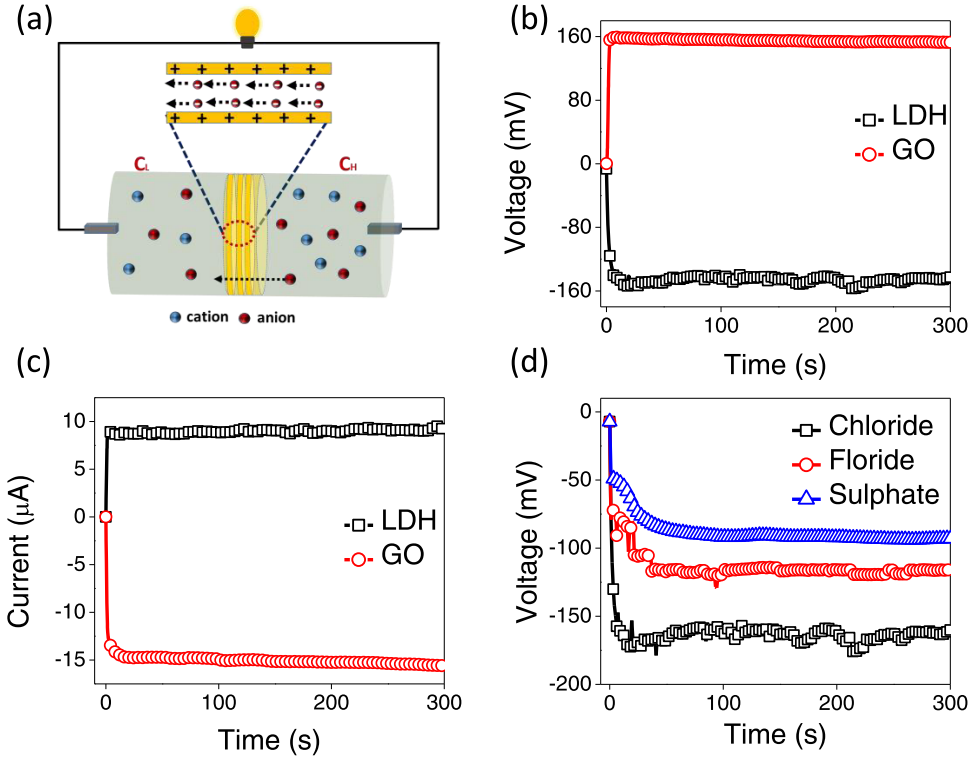

Figure 3. Charge selectivity of p-LDHM: (a) Schematic diagram of the device utilized for concentration gradient-based energy harvesting process. (b) Trans-membrane potential and (c) osmotic current generated with p-LDHM as a function of time. (d) Trans-membrane potential generated with p-LDHM as a function of time with increasing hydration radii of the anionic species; the corresponding hydration radii of chloride, fluoride, and sulfate are 0.33, 0.35, and 0.38 nm respectively. A 1000-fold concentration gradient was maintained by placing 10 mM KCl in the high-concentration chamber and 10 μM KCl in the low-concentration chamber, respectively, throughout all of the experiments.

was also measured with aqueous solutions of NaF and Na_2SO_4, as shown in Supporting Figure S3. As can be seen from Figure 2, conductivity values at the surface-charge-governed regime were found to be proportional to the hydration radius/bulk mobility of the anions. The counterion selectivity of p-LDHM was also verified by analyzing the samples under energy-dispersive X-ray (EDX) spectroscopy, as discussed in Supporting Figure S4. In brief, a strip of p-LDHM was soaked in 1 mM NaCl solution for 30 min, which was followed by drying in air for 6 h. The salt-soaked p-LDHM strip was mapped for different elements with EDX and is shown in Supporting Figure S4. The EDX map revealed the overwhelming presence of Cl^- compared to that of the Na^+.

Nanofluidic membrane with remarkable OH^- ion conductivity could find a large number of applications in areas like energy harvesting, charge transportation, and molecular sensing. To gain further insights into the mechanism of rapid OH^- transportation through the nanochannels of p-LDHM, hydroxide conductivity was measured as a function of temperature. The conductivity value (G) obtained using aqueous NaOH (10^{-4} M) solution as the electrolyte is plotted in the Arrhenius form (lnG vs 1/T). From the Arrhenius plot, the activation energy for the OH^- conduction was calculated to be 0.09 eV (Figure 2f). The small value of activation energy indicates a Grotthuss-like hopping of OH^- ions inside the LDH nanochannels.[38] In the Grotthuss-like hopping process, charge is transported through synchronized hopping of ions (OH^-) between the well-organized chains of water molecules in strict two dimensions.

In nanofluidic systems, the nature and concentration of ions present inside the channels are dictated by the polarity and density of charges on the channel walls. Therefore, it is important to determine the surface-charge density (σ_s) of the p-LDHM channels. The σ_s value calculated using the Grahame equation[39] (eq 1) was found to be ~2 mC·m^{-2}.

$$\sigma_s = \frac{\varepsilon \varepsilon_o \zeta}{\lambda_d} \tag{1}$$

In the Grahame equation, ε is the dielectric constant ε_o is the permittivity of vacuum, and λ_d is the Debye length calculated as $\frac{0.304}{\sqrt{I(\mathrm{M})}}$nm, where I (M) is the ionic strength in molarity and ζ is the zeta potential. The σ_s value obtained as such was used to determine the mobility (μ_-) of different anionic species in the p-LDHM channels using eq 2, which correlates ionic mobility and surface-charge densities to surface-charge-governed conductivity (G_s).[40]

$$G_s = 2\mu_- \sigma_s \frac{w}{l} \tag{2}$$

where w (0.040 mm) and l (20 mm) correspond to the width and length of the membrane, respectively. Remarkably, in the surface-charge-governed region, mobility values of all of the anionic species μ_- were calculated to be close to that of the bulk water, as shown in Supporting Figure S5.

To verify these experimental findings, the calculated σ_s value was used to determine the effective height (h_{eff}) of the p-LDHM nanochannels in aqueous environment. The h_{eff} value of the LDH nanochannels determined from the transition point concentration (C_t) of conductivity vs concentration plot was found to be 0.38 nm, which is very close to the one calculated from the powder XRD pattern (0.40 nm) of the

https://doi.org/10.1021/acs.jpcc.1c03118
J. Phys. Chem. C 2021, 125, 17939−17949

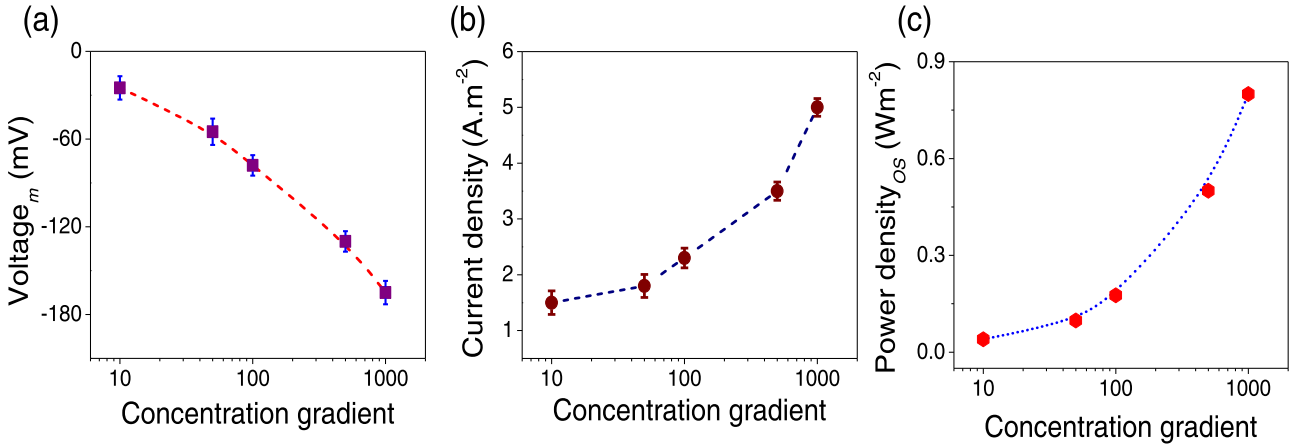

Figure 4. Osmotic energy conversion: (a) Trans-membrane potential, (b) current density defined as the total osmotic current divided by the area of the membrane in contact with the electrolyte (area of ionic interface ~2.5 mm^2), and (c) power density obtained with p-LDHM as a function of concentration gradient.

hydrated p-LDHM. For this calculation, C_t was obtained from the regime where the transport characteristics varied from surface-charge-governed regime to bulk-like behavior; details are shown in Supporting Figure S6. σ_s is connected to C_t by eq 3.[41,42]

$$h_{eff} = 10^{-3}\frac{\sigma_s}{eN_A C_t} \tag{3}$$

Further insights into the ion selectivity behavior of the p-LDHM were obtained by measuring the trans-membrane potential and trans-membrane current under a predefined concentration gradient. As shown in Figure 3a, the experimental setup employed for this measurement is composed of two compartments separated by a p-LDHM. The electrolyte concentration at one side of the membrane was fixed at 10 μM, while the concentration at the other side was increased from 100 μM to 10 mM. Two Ag/AgCl electrodes were inserted into the electrolyte solutions to measure the open-circuit voltage (V_{OC}) and short-circuit current (I_{SC}) across the p-LDHM. The V_{OC} measured as such consists of two parts, trans-membrane or simply membrane potential (V_m) and redox potential (V_{redox}). The membrane potential (V_m) has three contributions: the Donnan potentials at each edge of the nanopore and the diffusion potential attributes to the trans-membrane salinity gradient and greater mobility of cations over anions, while the redox potential (V_{redox}) is originated from the unequal potential drop at the electrode−solution interface.[43−46] The employment of Ag/AgCl electrodes with saturated KCl bridges offset the electrode potential, so V_{redox} can be ignored and hence the measured V_{OC} is attributed to the membrane potential (V_m) originating from the migration of counterions through the p-LDHM nanochannels along with the contribution of Donnan potentials at each edge of the electrolyte−nanpore interface.[26] The limit of the possible errors due to the leakage of additional ions from the salt bridge was estimated by measuring the conductivity of DI water in the presence and absence of the salt bridge as shown in Supporting Figure S7. Nevertheless, leakage of ions from the salt bridge to the electrochemical cell was found to be negligible (0.42 μM h^{-1}). Moreover, salt bridges were positioned at each side of the membrane, at a distance of 1.5 cm away from the membrane, and hence the error due to possible leakage will be self-correcting. Figure 3b,c compares the V_m and osmotic current (I_{OS}) of p-LDHM with that of negatively charged graphene oxide membrane (GO) under a 1000-fold concentration gradient. Under the identical experimental condition, V_m and I_{OS} of the p-LDHM (−144 mV) were measured to be opposite to that of the anionic GO membrane (+155 mV). The observed high value of V_m could have contributions from both Donnan and diffusion potential. Occurrence of an additional perm-selective diffusional process can make the membrane potential exceed its theoretically predicted maximum value of Donnan potential. In fact, development of high V_m values due to the combined effect of Donnan and diffusion potential is reported earlier.[47] The V_m of the LDH membrane was also measured with different electrolyte solutions (NaCl, NaF, Na_2SO_4; same cation but different anions) under 1000-fold trans-membrane concentration gradient. As can be seen from Figure 3d, the V_m values decrease with increasing hydration radii of the anionic species, confirming that the selective diffusion of anionic counterions through the p-LDHM has a significant contribution to the observed potential difference. With increasing hydration radii, the anionic species will face more hindrance in diffusing through the nanofluidic channels, and this slow crossover of anionic species will in turn reduce the output values of V_m.[48,49] The V_m values originating in the p-LDHM membrane are also used for the calculation of counterion transference number (t_-) by employing eq 4, assuming that the membrane transference numbers are constant throughout the membrane phase. Eq 4 for membrane potential (V_m) can be derived from the Donnan potentials and diffusion potential, which is summarized by Geise et al.[44]

$$V_m = (t_+ - t_-)\frac{RT}{F}\ln\frac{C_{High}}{C_{Low}} \tag{4}$$

The p-LDHM displayed a remarkable preference for the chloride anions with transference number (t_-) approaching 0.95 under 1000-fold concentration difference.

The high transport number and excellent nanofluidic transport of the pLDHM paved the way for harvesting electrical energy from salinity gradient. As shown in Figure 4a,b, both V_m and I_{OS} values of the pLDHM devices were found to be increasing with the increase in the concentration gradient. The osmotic power density for different concentration gradient was calculated according to eq 5,[26,50] and a remarkable 0.7 Wm^{-2} power density was achieved under a

https://doi.org/10.1021/acs.jpcc.1c03118
J. Phys. Chem. C 2021, 125, 17939−17949

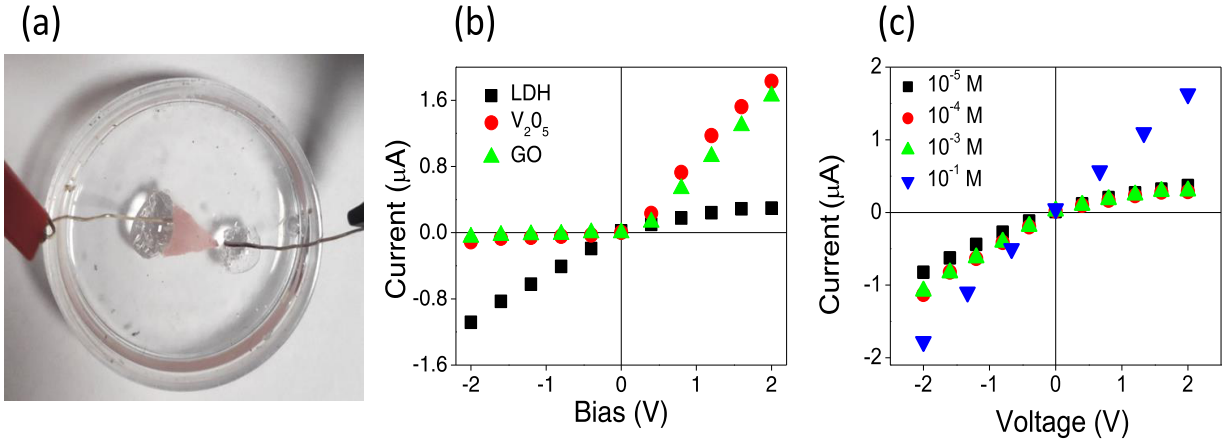

Figure 5. Ionic current rectification (ICR) via triangular p-LDHM device: (a) Digital image of the triangular nanofluidic device of p-LDHM. (b) *I*−*V* curves recorded with triangular p-LDHM device compared with that of GO and V_2O_5 devices. (c) ICR as a function of KCl concentration.

1000-fold concentration gradient of KCl electrolyte, as shown in Figure 4c.

$$P_{OS} = \frac{I_{OS} \times V_{OS}}{\text{Area}} \tag{5}$$

The total energy conversion efficiency or power conversion efficiency is defined as the ratio of the total/integrated power produced over time to the total Gibbs free energy supplied. The total energy conversion efficiency indicates the percentage of the chemical energy consumed within the RED stack, which is converted into electrical power. It is expressed as shown in eq 6[43]

$$\eta = \frac{\Delta E_m Q_t}{\Delta E_{ideal} Q_{t.ideal}} \tag{6}$$

where ΔE_{ideal} is the ideal equilibrium voltage, ΔE_m is the measured voltage, Q_t is the actual transferred charge, and $Q_{t,ideal}$ is the ideal transferred charge.

In the nanofluidic energy conversion device, power is harvested from the selective transport of either cations or anions and hence for the condition of maximum power generation, ΔE_m is further reduced from ΔE_{ideal} by a factor of 2. Now expressing the transferred charge in terms of anion-transferred number and applying the condition of maximum power generation, the maximum energy conversion efficiency (η_{max}) can be expressed as in shown in eq 7[51,52] and η_{max} was calculated to be ∼44% for a 1000-fold concentration difference of KCl electrolyte with our p-LDHM device.

$$n_{max} = \frac{1}{2}(2t_- - 1)^2 \tag{7}$$

It is clear from eq 7 that even with a perfect perm-selective membrane, the maximum energy efficiency of a nanofluidic osmotic energy generator is limited to only 50%. Therefore, fabrication of anion-selective nanofluidic membrane is of utmost interest where we can utilize both the complementary charge selective membrane in synchronization for achieving better performance in osmotic energy conversion.[43]

Nanofluidic devices of p-LDHM demonstrated an interesting shape-dependent ionic transport behavior. As shown in Figure 2b, nanofluidic devices of rectangular p-LDHM strips (symmetric) exhibit linear *I*−*V* curves. On a clear contrast, nanofluidic devices fabricated with triangular (asymmetric) p-LDHM strips displayed nonlinear *I*−*V* curves, where the current values in forward bias were found to be significantly higher than in the reversed bias (shown in Figure 5b). This phenomenon of exhibiting diode-like behavior in asymmetric nanopore is known as the ionic current rectification (ICR). The origin of ICR in the asymmetric nanofluidic channel is attributed to the preferential migration of ionic species in one direction and restricting the same in the opposite direction. Under such conditions, the ionic current recorded at forward bias (+V) is found to be higher than the one recorded at an equal voltage of reverse bias (−V). Such ion-selective behavior is common in biological ion pumps, and they play vital roles in maintaining ionic concentration gradient across the cellular membrane. Inspired by the biological systems, ICR behavior was repeated in several artificial systems, like the conical nanopores,[53] longitudinal hetero-structured nanotubes,[54] homogeneous nanochannels with asymmetric bath concentrations,[55] and triangular membranes of reconstructed graphene oxide[56] and vanadium pentoxide.[10] The *I*−*V* curve shown in Figure 5b (black line) was recorded through an isosceles triangle cut from p-LDHM (15 mm (altitude) × 5 mm (base) × 0.030 mm (thickness)), and aqueous solution of KCl (10^{-4} M) was placed on both the reservoirs. The nonlinearity of the *I*−*V* curve clearly reveals that the current values at positive bias are significantly lower than that of the negative bias of similar magnitude. The *I*−*V* curve of the triangular p-LDHM strip is also compared with that of GO and V_2O_5 strips. In all of these devices, bias was applied at the base side of the triangle. Remarkably, the direction of ICR in p-LDHM was found to be opposite to that of GO and V_2O_5 triangle, due to the opposite polarity of charges in the channel walls. The ICR ratio (ratio of the magnitude of the current recorded at +1 and −1 V) for triangular p-LDHM with 10^{-4} M KCl was found to be 3 (Figure 5c). In the surface-charge-governed regime (10^{-5}−10^{-3} M), the ICR ratio was found to be independent of salt concentration. However, in the high-concentration regime (10^{-2}−1 M), the ICR value decreases with increasing salt concentrations. This observation indicates the origin of ICR to be the unipolar conductivity of p-LDHM in the surface-charge-governed region. In addition to surface-charge-governed conductivity, another requisite parameter for achieving ICR is the geometrical asymmetry. ICR was not observed in rectangular devices even in the surface-charge-governed region.

https://doi.org/10.1021/acs.jpcc.1c03118
J. Phys. Chem. C 2021, 125, 17939−17949

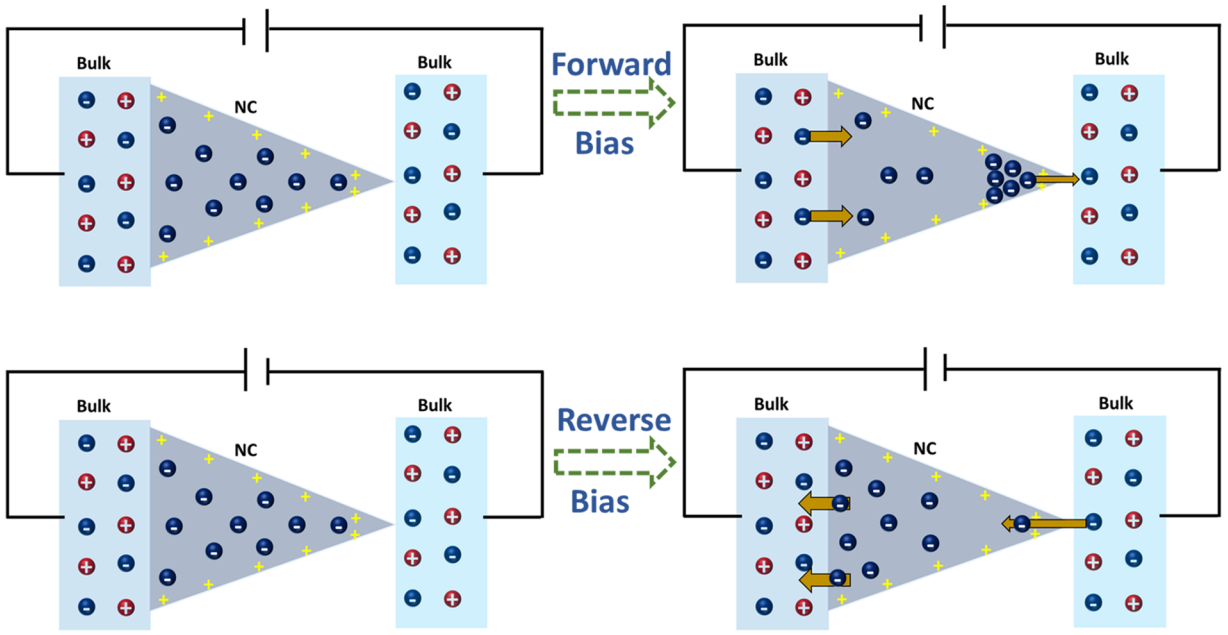

Figure 6. Mechanism of ICR: Schematic illustration of ICR with 2D triangular nanochannel of p-LDHM.

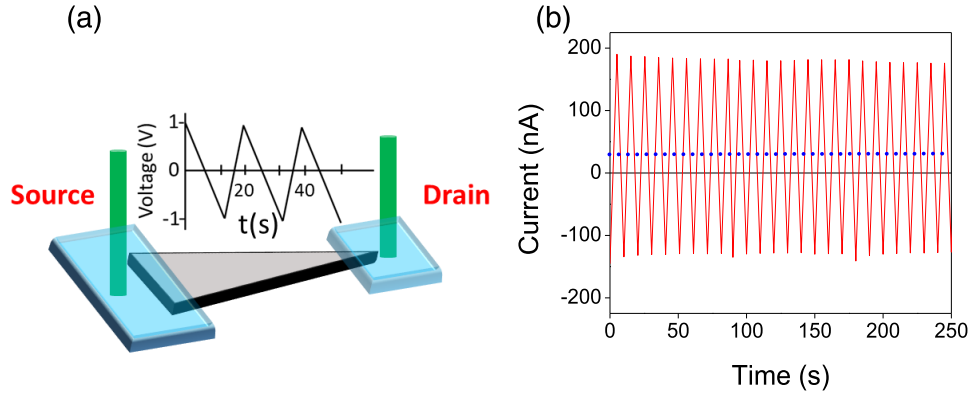

Figure 7. Ion pumping by triangular p-LDHM nanofluidic device: (a) Schematic representation of the experimental setup utilized for ion pumping under fluctuating electric field with a mean value of zero. (b) Plot of current as a function of time recorded under a fluctuating electric field of zero means (between +1 and −1 V) against a 1000-fold concentration gradient.

The probable mechanism of ICR in triangular p-LDHM is illustrated in the schematic of Figure 6. In the surface-charge-governed regime (10^{-2}–10^{-6} M), the overlapping EDL rejects the co-ions and builds up an elevated concentration of counterions (Cl^- ions), which is significantly higher than that of the reservoirs. Due to the geometrical constraints, the total current flowing through the p-LDHM triangle in any direction is determined by the number of ions flowing through the tip of the triangle. On forward bias, Cl^- ions residing inside the nanochannel flow from the p-LDHM triangle to the bulk reservoir through the tip side. On this bias, ions flow from a region of higher ionic concentration to a reservoir of lower concentration, and hence produced higher ionic flux (Figure 6, "forward bias"). Similarly, at the reverse bias, ions flow from a region of lower ionic concentration (from the reservoir) to a region of higher ionic concentration (at the p-LDHM triangle), which leads to lower ionic flux. Moreover, the higher ionic current in the forward bias is supported by a larger entrance (base)/exit (tip) ratio. In contrast, in the reverse bias, anions experience a much lower entrance (base)/exit (tip) ratio.

The ion-rectifying nature of the triangular p-LDHM can also be exploited as an ion pump to push anions against the concentration gradient under a fluctuating external potential with a mean value of zero, where the applied potential was varied between +1 and −1 V, maintaining a mean voltage value of zero and the corresponding current response was plotted as a function of time. A schematic of the triangular device fabricated for attaining the active anion pumping effect is shown in Figure 7 a. To verify the anion pumping behavior, both the reservoirs were filled with aqueous KCl solution of different concentrations and the concentrations of the base and tip reservoirs of a triangular p-LDHM device were fixed at 10^{-5} and 10^{-3} M, respectively. The electric field between the reservoirs was periodically varied between +1 and −1 V through Ag/AgCl electrodes placed at the reservoirs. The current response of the triangular device under the influence of fluctuating electric field was recorded as a function of time. As shown in Figure 7b, for a 1000-fold concentration difference (10^{-2}–10^{-5} M), a positive average current of 2.5×10^{-8} A (dotted blue line) was observed. It indicates a net flow of the Cl^- ions in the uphill direction (against the concentration

https://doi.org/10.1021/acs.jpcc.1c03118
J. Phys. Chem. C 2021, 125, 17939−17949

gradient), under the fluctuating electric field. The uphill migration of ions was also confirmed by measuring the initial and final concentrations of the electrolytes in the source reservoir. The magnitude of ion pumping was further enhanced by fabricating a device with six triangular membranes (Supporting Figure S8a), where all of the drain and source reservoirs are interconnected. After applying a fluctuating electric field (between +1 and −1 V) with zero mean, for 3 min, the initial and final conductivities of the electrolytes in the source reservoirs were measured from the slopes of the $I-V$ curves (Supporting Figure S8b). From the difference in the conductivity values, the concentration difference of the ions in the source reservoir before and after ion pumping (for 3 min) was found to be 2.23×10^{-6} M; details of the calculation are presented in Supporting Table 1. The decreasing concentration of the ions in the low-concentration reservoir after applying fluctuating electric field confirms the ion pumping effect of triangular p-LDHM against the concentration gradient.

CONCLUSIONS

In conclusion, we have demonstrated the fabrication of a nanofluidic ion pump using reconstructing exfoliated layers of CoAl LDH in the form of a membrane. The atomically thin space between the layers CoAl LDH provided a unique platform to study anion transport characteristics under extreme confinement. Inherent anion selectivity of p-LDHM can also be utilized for converting the salinity gradient into electrical energy up to 0.7 Wm^{-2}. Nanofluidic devices of p-LDHM displayed a shape-dependent ionic transport characteristic. While the rectangular pieces of membranes exhibit linear $I-V$ curves, in the surface-charged-governed regime, the triangularly cut p-LDHM displays a diode-like ionic current rectification behavior. The ICR behavior of triangular p-LDHM was exploited to pump anions against the concentration gradient under fluctuating external potential with a mean value of zero. The ease of fabrication of the bio-inspired anion pump from p-LDHM would help us to fabricate devices for futuristic applications in areas like bio-sensing, environmental studies, and energy harvesting. Systematic investigation of the ion transport characteristic through the interlayer spacing of LDH could not only help in understanding the functioning of the biological systems but also can improve the performance of devices in diverse areas like water purification, anion sensing, osmotic energy harvesting, and catalysis.

ASSOCIATED CONTENT

Supporting Information

The Supporting Information is available free of charge at https://pubs.acs.org/doi/10.1021/acs.jpcc.1c03118.

ζ-Potential measurement of CoAl LDH dispersion, comparison of PXRD pattern of p-LDHM in wet and dry states, surface-charge-governed ion transport through p-LDHM on exposure to different concentrations of NaF and Na_2SO_4 electrolyte, EDX spectra of p-LDHM soaked in NaCl electrolyte, comparison of ionic mobilities of different anionic species through p-LDHM, plot of the determination of transition point concentration (C_t), enhancement of ion pumping with a scaled-up p-LDHM device, and comparison of ionic concentration in the source reservoir before and after ion pumping (PDF)

AUTHOR INFORMATION

Corresponding Author

Kalyan Raidongia − *Department of Chemistry, Indian Institute of Technology Guwahati, Guwahati 781039 Assam, India; Centre for Nanotechnology, Indian Institute of Technology Guwahati, Guwahati 781039 Assam, India;* orcid.org/0000-0001-7829-7498; Email: k.raidongia@iitg.ac.in

Authors

Tukhar Jyoti Konch − *Department of Chemistry, Indian Institute of Technology Guwahati, Guwahati 781039 Assam, India*

Trisha Dutta − *Department of Chemistry, Indian Institute of Technology Guwahati, Guwahati 781039 Assam, India*

Arindom Bikash Neog − *Department of Chemistry, Indian Institute of Technology Guwahati, Guwahati 781039 Assam, India*

Raktim Gogoi − *Department of Chemistry, Indian Institute of Technology Guwahati, Guwahati 781039 Assam, India*

Complete contact information is available at: https://pubs.acs.org/10.1021/acs.jpcc.1c03118

Author Contributions

T.J.K. and T.D. contributed equally to this work. K.R. conceived the concept and designed the experiments. T.J.K., T.D., A.B.N., and R.G. performed the experiments and analyzed the data. K.R. and T.J.K. wrote the paper, with input from all of the authors. All authors approved the final version of the manuscript.

Notes

The authors declare no competing financial interest.

ACKNOWLEDGMENTS

K.R. acknowledges EMR grant of CSIR-India (01(2984)/19/EMR-II) and Core Research Grant of SERB (CRG/2020/002943) of the Science and Engineering Research Board (SERB), India, for financial support. All of the authors thank CIF-IIT Guwahati, DST-FIST-Chemistry at IIT Guwahati for the help with sample characterizations. T.D. and T.J.K. are grateful to IITG for Ph.D. fellowships.

REFERENCES

(1) Decker, K.; Page, M.; Aksimentiev, A. Nanoscale Ion Pump Derived from a Biological Water Channel. *J. Phys. Chem. B* **2017**, *121*, 7899−7906.

(2) Reyes, N.; Gadsby, D. C. Ion Permeation through the Na^+, K^+-ATPase. *Nature* **2006**, *443*, 470−474.

(3) Morth, J. P.; Pedersen, B. P.; Buch-Pedersen, M. J.; Andersen, J. P.; Vilsen, B.; Palmgren, M. G.; Nissen, P. A Structural Overview of the Plasma Membrane Na^+, K^+-ATPase and H^+-ATPase Ion Pumps. *Nat. Rev. Mol. Cell Biol.* **2011**, *12*, 60−70.

(4) Pedersen, B. P.; Buch-Pedersen, M. J.; Morth, J. P.; Palmgren, M. G.; Nissen, P. Crystal Structure of the Plasma Membrane Proton Pump. *Nature* **2007**, *450*, 1111−1114.

(5) Slayman, C. L.; Long, W. S.; Lu, C.-H. Y. The Relationship between ATP and an Electrogenic Pump in the Plasma Membrane of Neurospora Crassa. *J. Membr. Biol.* **1973**, *14*, 305−338.

(6) Verma, A. K.; Filoteo, A. G.; Stanford, D. R.; Wieben, E. D.; Penniston, J. T.; Strehler, E. E.; Fischer, R.; Heim, R.; Vogel, G.; Mathews, S.; et al. Complete Primary Structure of a Human Plasma Membrane Ca^{2+} Pump. *J. Biol. Chem.* **1988**, *263*, 14152−14159.

(7) Zhang, Z.; Kong, X.-Y.; Xie, G.; Li, P.; Xiao, K.; Wen, L.; Jiang, L. "Uphill" cation transport: A Bioinspired Photo-Driven Ion Pump. *Sci. Adv.* **2016**, *2*, No. 1600689.
(8) Xiao, K.; Chen, L.; Chen, R.; Heil, T.; Lemus, S. D. C.; Fan, F.; Wen, L.; Jiang, L.; Antonietti, M. Artificial Light-driven Ion Pump for Photoelectric Energy Conversion. *Nat. Commun.* **2019**, *10*, No. 74.
(9) Yang, J.; Liu, P.; He, X.; Hou, J.; Feng, Y.; Huang, Z.; Yu, L.; Li, L.; Tang, Z. Photodriven Active Ion Transport Through a Janus Microporous Membrane. *Angew. Chem., Int. Ed.* **2020**, *59*, 6244−6248.
(10) Gogoi, R. K.; Neog, A. B.; Konch, T. J.; Sarmah, N.; Raidongia, K. A Two-Dimensional Ion-Pump of a Vanadium Pentoxide Nanofluidic Membrane. *J. Mater. Chem. A* **2019**, *7*, 10552−10560.
(11) Rabinowitz, J.; Cohen, C.; Shepard, K. L. An Electrically Actuated, Carbon-Nanotube-Based Biomimetic Ion Pump. *Nano Lett.* **2020**, *20*, 1148−1153.
(12) Wu, C.; Xiao, T.; Tang, J.; Zhang, Q.; Liu, Z.; Liu, J.; Wang, H. Biomimetic Temperature-Gated 2D Cationic Nanochannels for Controllable Osmotic Power Harvesting. *Nano Energy* **2020**, *76*, No. 105113.
(13) Zhang, Z.; Kong, X. Y.; Xiao, K.; Liu, Q.; Xie, G.; Li, P.; Ma, J.; Tian, Y.; Wen, L.; Jiang, L. Engineered Asymmetric Heterogeneous Membrane: A Concentration-Gradient-Driven Energy Harvesting Device. *J. Am. Chem. Soc.* **2015**, *137*, 14765−14772.
(14) Raidongia, K.; Huang, J. Nanofluidic Ion Transport through Reconstructed Layered Materials. *J. Am. Chem. Soc.* **2012**, *134*, 16528−16531.
(15) Mouterde, T.; Keerthi, A.; Poggioli, A.; Dar, S.; Siria, A.; Geim, A.; Bocquet, L.; Radha, B. Molecular Streaming and Its Voltage Control in Ångström-Scale Channels. *Nature* **2019**, *567*, 87−90.
(16) Saha, K.; Deka, J.; Raidongia, K. Energy from the Nanofluidic Transport of Water through Nanochannels between Packed Silica Spheres. *ACS Appl. Nano Mater.* **2019**, *2*, 5850−5856.
(17) Huang, H.; Ying, Y.; Peng, X. Graphene Oxide Nanosheet: An Emerging Star Material for Novel Separation Membranes. *J. Mater. Chem. A* **2014**, *2*, 13772−13872.
(18) Chimene, D.; Alge, D. L.; Gaharwar, A. K. Two-Dimensional Nanomaterials for Biomedical Applications: Emerging Trends and Future Prospects. *Adv. Mater.* **2015**, *27*, 7261−7284.
(19) Homaeigohar, S.; Elbahri, M. Graphene Membranes for Water Desalination. *NPG Asia Mater.* **2017**, *9*, No. e427.
(20) Min, S. K.; Kim, W. Y.; Cho, Y.; Kim, K. S. Fast DNA Sequencing with a Graphene-Based Nanochannel Device. *Nat. Nanotechnol.* **2011**, *6*, 162−165.
(21) Qin, S.; Liu, D.; Wang, G.; Portehault, D.; Garvey, C. J.; Gogotsi, Y.; Lei, W.; Chen, Y. High and Stable Ionic Conductivity in 2D Nanofluidic Ion Channels Between Boron Nitride Layers. *J. Am. Chem. Soc.* **2017**, *139*, 6314−6320.
(22) Shao, J. J.; Raidongia, K.; Koltonow, A. R.; Huang, J. Self-Assembled Two-Dimensional Nanofluidic Proton Channels with High Thermal Stability. *Nat. Commun.* **2015**, *6*, No. 7602.
(23) Deng, M.; Kwac, K.; Li, M.; Jung, Y.; Park, H. G. Stability, Molecular Sieving, and Ion Diffusion Selectivity of a Lamellar Membrane from Two-Dimensional Molybdenum Disulfide. *Nano Lett.* **2017**, *17*, 2342−2348.
(24) Zhang, Z.; Yang, S.; Zhang, P.; Zhang, J.; Chen, G.; Feng, X. Mechanically Strong MXene/Kevlar Nanofiber Composite Membranes as High Performance Nanofluidic Osmotic Power Generators. *Nat. Commun.* **2019**, *2*, No. 2920.
(25) Xiao, K.; Giusto, P.; Wen, L.; Jiang, L.; Antonietti, M. Nanofluidic Ion Transport and Energy Conversion through Ultrathin Free-Standing Polymeric Carbon Nitride Membranes. *Angew. Chem., Int. Ed.* **2018**, *57*, 10123−10126.
(26) Ji, J.; Kang, Q.; Zhou, Y.; Feng, Y.; Chen, X.; Yuan, J.; Guo, W.; Wei, Y.; Jiang, L. Osmotic Power Generation with Positively and Negatively Charged 2D Nanofluidic Membrane Pairs. *Adv. Funct. Mater.* **2017**, *27*, No. 1603623.
(27) Wu, Q.-Y.; Wang, C.; Wang, R.; Chen, C.; Gao, J.; Dai, J.; Liu, D.; Lin, Z.; Hu, L. Salinity-Gradient Power Generation with Ionized Wood Membranes. *Adv. Energy Mater.* **2019**, *10*, No. 1902590.
(28) Ding, L.; Xiao, D.; Lu, Z.; Deng, J.; Wei, Y.; Caro, J.; Wang, H. Oppositely Charged $Ti_3C_2T_x$ MXene Membranes with 2D Nanofluidic Channels for Osmotic Energy Harvesting. *Angew. Chem., Int. Ed.* **2020**, *59*, 8720−8726.
(29) Song, X.; Zambare, R. S.; Qi, S.; Sowrirajalu, B. N.; Selvaraj, A. P. J.; Tang, C. Y.; Gao, C. Charge-Gated Ion Transport Through Polyelectrolyte Intercalated Amine Reduced Graphene Oxide Membranes. *ACS Appl. Mater. Interfaces* **2017**, *9*, 41482−41495.
(30) Konch, T. J.; Gogoi, R. K.; Gogoi, A.; Saha, K.; Deka, J.; Reddy, K. A.; Raidongia, K. Nanofluidic Transport Through Humic Acid Modified Graphene Oxide Nanochannels. *Mater. Chem. Front.* **2018**, *2*, 1647−1654.
(31) He, X.; Cao, L.; He, G.; Zhao, A.; Mao, X.; Huang, T.; Li, Y.; Wu, H.; Sun, J.; Jiang, Z. A Highly Conductive and Robust Anion Conductor Obtained via Synergistic Manipulation in Intra- and Inter-Laminate of Layered Double Hydroxide Nanosheets. *J. Mater. Chem. A* **2018**, *6*, 10277−10285.
(32) Sun, P.; Ma, R.; Ma, W.; Wu, J.; Wang, K.; Sasaki, T.; Zhu, H. Highly Selective Charge-Guided Ion Transport Through a Hybrid Membrane Consisting of Anionic Graphene Oxide and Cationic Hydroxide Nanosheet Superlattice Units. *NPG Asia Mater.* **2008**, *8*, No. e259.
(33) Sun, P.; Ma, R.; Bai, X.; Wang, K.; Zhu, H.; Sasaki, T. Single-Layer Nanosheets with Exceptionally High and Anisotropic Hydroxyl Ion Conductivity. *Sci. Adv.* **2017**, *3*, No. e1602629.
(34) Sun, J.; Li, P.; Qu, J.; Lu, X.; Xie, Y.; Gao, F.; Li, Y.; Gang, M.; Feng, Q.; Liang, H.; et al. Electricity Generation from a Ni-Al Layered Double Hydroxide-Based Flexible Generator Driven by Natural Water Evaporation. *Nano Energy* **2019**, *57*, 269−278.
(35) Liu, Z.; Ma, R.; Osada, M.; Iyi, N.; Ebina, Y.; Takada, K.; Sasaki, T. Synthesis, Anion Exchange, and Delamination of Co-Al Layered Double Hydroxide: Assembly of the Exfoliated Nanosheet/Polyanion Composite Films and Magneto-Optical Studies. *J. Am. Chem. Soc.* **2006**, *128*, 4872−4880.
(36) Liang, J.; Ma, R.; Iyi, N.; Ebina, Y.; Takada, K.; Sasaki, T. Topochemical Synthesis, Anion Exchange, and Exfoliation of Co-Ni Layered Double Hydroxides: A Route to Positively Charged Co-Ni Hydroxide Nanosheets with Tunable Composition. *Chem. Mater.* **2010**, *22*, 371−378.
(37) Song, F.; Hu, X. Exfoliation of Layered Double Hydroxides for Enhanced Oxygen Evolution Catalysis. *Nat. Commun.* **2014**, *5*, No. 4477.
(38) Ordinario, D. D.; Phan, L.; Walkup, W. G., IV; Jocson, J. M.; Karshalev, E.; Hüsken, N.; Gorodetsky, A. A. Bulk Protonic Conductivity in a Cephalopod Structural Protein. *Nat. Chem.* **2014**, *6*, 596−602.
(39) Butt, H. J.; Graf, K.; Kappl, M. *Physics and Chemistry of Interfaces*, 3rd ed.; Wiely-VCH: Weinheim, Germany, 2006.
(40) Duan, C.; Majumdar, A. Anomalous Ion Transport in 2-nm Hydrophilic Nanochannels. *Nat. Nanotechnol.* **2010**, *5*, 848−852.
(41) Schoch, R. B.; Renaud, P. Ion Transport through Nanoslits Dominated by the Effective Surface Charge. *Appl. Phys. Lett.* **2005**, *86*, No. 253111.
(42) Konch, T. J.; Bora, A. P.; Raidongia, K. Disposable Fluidic Devices of Bionanochannels for Enzymatic Monitoring and Energy Harvesting. *ACS Appl. Bio Mater.* **2019**, *2*, 2549−2556.
(43) Wang, L.; Wang, Z.; Patel, S. K.; Lin, S.; Elimelech, M. Nanopore-Based Power Generation from Salinity Gradient: Why It Is Not Viable. *ACS Nano* **2021**, *15*, 4093−4107.
(44) Geise, G. M.; Cassady, H. J.; Paul, D. R.; Logan, B. E.; Hickner, M. A. Specific Ion Effects on Membrane Potential and the Permselectivity of Ion Exchange Membranes. *Phys. Chem. Chem. Phys.* **2014**, *16*, 21673−21681.
(45) Schoch, R. B.; Han, J.; Renaud, P. Transport Phenomena in Nanofluidics. *Rev. Mod. Phys.* **2008**, *80*, 839−883.

https://doi.org/10.1021/acs.jpcc.1c03118
J. Phys. Chem. C 2021, 125, 17939−17949

(46) Kim, D.-K.; Duan, C.; Chen, Y.-F.; Majumdar, A. Power Generation from Concentration Gradient by Reverse Electrodialysis in Ion-Selective Nanochannels. *Microfluid. Nanofluid.* **2010**, *9*, 1215−1224.
(47) Ahualli, S.; Fernandez, M. M.; Iglesias, G.; Jimenez, M. L.; Liu, F.; Wagterveld, M.; Delgado, A. V. Effect of solution composition on the energy production by capacitive mixing in membrane-electrode assembly. *J. Phys. Chem. C* **2014**, *118*, 15590−15599.
(48) Zwolak, M.; Lagerqvist, J.; Di Ventra, M. Quantized Ionic Conductance in Nanopores. *Phys. Rev. Lett.* **2009**, *103*, No. 128102.
(49) Wang, Y.; Zhang, H.; Kang, Y.; Zhu, Y.; Simon, G. P.; Wang, H. Voltage-Gated Ion Transport in Two-Dimensional Sub-1 nm Nanofluidic Channels. *ACS Nano* **2019**, *13*, 11793−11799.
(50) Lee, K. H.; Park, H.; Eom, W.; Kang, D. J.; Noh, S. H.; Han, T. H. Graphene Quantum Dots/Graphene Fiber Nanochannels for Osmotic Power Generation. *J. Mater. Chem. A* **2019**, *7*, 23727−23732.
(51) Hong, S.; Ming, F.; Shi, Y.; Li, R.; Kim, I. S.; Tang, C. Y.; Alshareef, H. N.; Wang, P. Two-Dimensional $Ti_3C_2T_x$ MXene Membranes as Nanofluidic Osmotic Power Generators. *ACS Nano* **2019**, *13*, 8917−8925.
(52) Xin, W.; Zhang, Z.; Huang, X.; Hu, Y.; Zhou, T.; Zhu, C.; Kong, X.-Y.; Jiang, L.; Wen, L. High-Performance Silk-Based Hybrid Membranes Employed for Osmotic Energy Conversion. *Nat. Commun.* **2019**, *10*, No. 3876.
(53) Kasianowicz, J. J.; Brandin, E.; Branton, D.; Deamer, D. W. Characterization of Individual Polynucleotide Molecules Using a Membrane Channel. *Proc. Natl. Acad. Sci. U.S.A.* **1996**, *93*, 13770−13773.
(54) Yan, R.; Liang, W.; Fan, R.; Yang, P. Nanofluidic Diodes Based on Nanotube Heterojunctions. *Nano Lett.* **2009**, *9*, 3820−3825.
(55) Cheng, L.-J.; Guo, L. J. Rectified Ion Transport through Concentration Gradient in Homogeneous Silica Nanochannels. *Nano Lett.* **2007**, *7*, 3165−3171.
(56) Gao, J.; Koltonow, A. R.; Raidongia, K.; Beckerman, B.; Boon, N.; Luijten, E.; De La Cruz, M. O.; Huang, J. Kirigami Nanofluidics. *Mater. Chem. Front.* **2018**, *2*, 475−482.

https://doi.org/10.1021/acs.jpcc.1c03118
J. Phys. Chem. C 2021, 125, 17939−17949